Biomaterials 52 (2015) 507–516

Contents lists available at ScienceDirect

Biomaterials

journal homepage: www.elsevier.com/locate/biomaterials

Uniform brain tumor distribution and tumor associated macrophage targeting of systemically administered dendrimers

Fan Zhang [a, b, 1], Panagiotis Mastorakos [a, 1], Manoj K. Mishra [a], Antonella Mangraviti [c], Lee Hwang [c], Jinyuan Zhou [d], Justin Hanes [a, c, e, f], Henry Brem [a, c, e], Alessandro Olivi [c], Betty Tyler [c, 2], Rangaramanujam M. Kannan [a, b, f, 2, *]

[a] Center for Nanomedicine at the Wilmer Eye Institute, Department of Ophthalmology, Johns Hopkins University School of Medicine, Baltimore, MD 21231, United States
[b] Department of Materials Science and Engineering, Johns Hopkins University, Baltimore, MD 21218, United States
[c] Department of Neurosurgery, Johns Hopkins University School of Medicine, Baltimore, MD 21287, United States
[d] F.M. Kirby Research Center for Functional Brain Imaging, Kennedy Krieger Institute, Baltimore, MD 21205, United States
[e] Department of Biomedical Engineering, Johns Hopkins University School of Medicine, Baltimore, MD 21205, United States
[f] Department of Chemical and Biomolecular Engineering, Johns Hopkins University, Baltimore, MD 21218, United States

ARTICLE INFO

Article history:
Received 21 November 2014
Received in revised form
11 February 2015
Accepted 13 February 2015
Available online 18 March 2015

Keywords:
PAMAM dendrimer
Glioblastoma
Tumor penetration
Tumor associated macrophages
Biodistribution
Blood-brain barrier

ABSTRACT

Effective blood–brain tumor barrier penetration and uniform solid tumor distribution can significantly enhance therapeutic delivery to brain tumors. Hydroxyl-functionalized, generation-4 poly(amidoamine) (PAMAM) dendrimers, with their small size, near-neutral surface charge, and the ability to selectively localize in cells associated with neuroinflammation may offer new opportunities to address these challenges. In this study we characterized the intracranial tumor biodistribution of systemically delivered PAMAM dendrimers in an intracranial rodent gliosarcoma model using fluorescence-based quantification methods and high resolution confocal microscopy. We observed selective and homogeneous distribution of dendrimer throughout the solid tumor (~6 mm) and peritumoral area within fifteen minutes after systemic administration, with subsequent accumulation and retention in tumor associated microglia/macrophages (TAMs). Neuroinflammation and TAMs have important growth promoting and pro-invasive effects in brain tumors. The rapid clearance of systemically administered dendrimers from major organs promises minimal off-target adverse effects of conjugated drugs. Therefore, selective delivery of immunomodulatory molecules to TAM, using hydroxyl PAMAM dendrimers, may hold promise for therapy of glioblastoma.

1. Introduction

Malignant glioma is the most common and most aggressive primary brain tumor [1] and despite the advances in treatment, the median survival remains at 16.4 months [2]. Key challenges faced in the development of effective therapies relate to (a) the ability of systemically delivered chemotherapeutic agents to penetrate the impaired blood–brain tumor barrier (BBTB) and provide coverage across the entire solid tumor [3] and (b) the ability to target specific cells. Although small molecule-based therapeutics can effectively distribute within the tumor tissue, they are limited by rapid tumor clearance [4] and off-target extravasation, potentially leading to adverse effects [3]. Recent advances in nanotechnology have provided selective tumor accumulation. However, the size of most nanoparticles limits extravasation and tumor penetration, thus limiting homogeneous solid tumor coverage [3,5]. Careful tuning of particle size and surface charge has been attempted in order to enhance the nanoparticle distribution profile in subcutaneous tumors [6–9]. Unfortunately, achieving homogeneous coverage of orthotopic brain tumors has been proven even more challenging. This may be attributed to the lower permeability of the BBTB compared to the blood-tumor barrier (BTB) in a subcutaneous tumor, the heterogeneous intervascular spaces and the high

* Corresponding author. Center for Nanomedicine at the Wilmer Eye Institute, Department of Ophthalmology, Johns Hopkins University School of Medicine, Baltimore, MD 21231, United States. Tel.: +1 443 287 8634; fax: +1 443 287 8635.
E-mail address: krangar1@jhmi.edu (R.M. Kannan).
[1] Contributed equally.
[2] Equal senior authors.

http://dx.doi.org/10.1016/j.biomaterials.2015.02.053
0142-9612/

interstitial pressure in brain tumors. Although, some strategies have attempted nanoparticle delivery through the BBTB via absorptive uptake; passive diffusion through the leaky BBTB fenestrations has only been demonstrated with molecules smaller than 20 nm [10–13] and unhindered diffusion through the BBTB has been achieved with molecules of 7 nm [14], thus limiting the relevance of most nanoparticle-based therapeutics.

Hydroxyl-terminated generation 4 poly(amidoamine) (PAMAM G4-OH) dendrimer is a highly tailorable branched macromolecule with a hydrodynamic size (~4 nm) smaller than conventional nanoparticles and near-neutral surface charge (ζ-potential: +4.5 ± 0.1 mV), physicochemical attributes that may allow for effective blood-brain barrier (BBB) [15] and tumor extra cellular matrix (ECM) penetration [16]. We have previously shown that, without the use of targeting ligands, these dendrimers can target activated microglia/macrophages after passing the impaired BBB in a rabbit model of cerebral palsy [17]. This targeted accumulation resulted in a significant efficacy when the dendrimer was conjugated to N-acetylcysteine [17]. In glioma, tumor associated microglia/macrophages (TAM) have been shown to participate in tumor growth, tumor invasion, angiogenesis and immune system evasion [18]. A variety of microglia/macrophage modulating molecules has been shown to decrease glioma progression and increase survival in preclinical studies [19–22]. Therefore, nanoparticle targeting of TAM has been explored, through the use of different ligands [23–26].

We investigated the use of PAMAM G4-OH dendrimer as a promising therapeutic vehicle for the treatment of malignant glioma. A recently developed fluorescence-based 'quantification' approach and high resolution confocal microscopy were combined to investigate the kinetics, biodistribution and clearance of these dendrimers in a 9L gliosarcoma intracranial tumor model. We also characterized the dendrimer's intrinsic ability to selectively target TAM.

2. Materials and methods

2.1. Materials and reagents

The following agents were purchased: hydroxyl terminated ethylenediamino-core PAMAM dendrimer (referred to as dendrimer throughout, unless otherwise specified) (Dendritech, Midland, MI), Methanol (HPLC grade), DMF (HPLC grade), stainless steel beads (Fisher Scientific, Waltham, MA); and Cyanine 5 (Cy5) (GE Healthcare Life Science, Pittsburgh, PA). For confocal microscopy: nuclei counterstain, 4′,6-diamidino-2-phenylindole, dihydrochloride (DAPI), Alexa Fluor® 594 Goat Anti-Rabbit IgG (H + L) Antibody (Molecular Probes, Eugene, Oregon); Fluorescent mounting media (Dako, Santa Clara, CA); Anti-Iba1, Rabbit (Wako, Osaka, Japan); Lectin from Bandeiraea simplicifolia (BSI-B4) (Sigma–Aldrich, St. Louis, MO); Anti-GFAP 488 (eBioscience, San Diego, CA); Fluorescein isothiocyanate–dextran (FITC-dextran), molecular weight 70,000 Da (Sigma Aldrich, St. Louis, MO).

2.2. Synthesis of dendrimer Cy5 (D-Cy5) conjugates

D-Cy5 was prepared through two steps following a previously published method [27]. Briefly, hydroxyl-terminated PAMAM dendrimer was surface-modified with amine groups to make a bifunctional dendrimer. We used 6-(Fmoc-amino) caproic acid to produce a Fmoc-protected bifunctional dendrimer intermediate that was eventually de-protected by re-dissolving in a mixture of piperidine/DMF. Cy5 dye with N-hydroxysuccinimide monoester was reacted with amine groups on the surface of bifunctional dendrimer. The 'crude' products were further extensively purified by dialysis. The final D-Cy5 conjugate was characterized using 1H NMR, high-performance liquid chromatography (HPLC) and gel permeation chromatography (GPC). The conjugate was stored as a solid powder at −20 °C and reconstituted at 10 mg/mL with sterile 0.9% NaCl solution on the day of administration.

2.3. Tumor inoculation

Female Fischer 344 rats, weighing 125–175 g each (Harlan Bioproducts, Indiana, IN), were housed in standard facilities and given free access to food and water. 9L gliosarcoma intracranial implantation was performed as previously described [28]. Briefly, the 9L gliosarcoma (obtained from the Brain Tumor Research Center, UCSF, San Francisco, CA) maintained in the flank of F344, was surgically excised sectioned into 1 mm^3 pieces and placed in sterile 0.9% NaCl solution on ice for intracranial implantation. Rats were anesthetized and a midline scalp incision was made to identify the sagittal and coronal sutures. A burr hole was made 3 mm lateral to the sagittal suture and 5 mm posterior to the coronal suture. The dura was incised, and using a surgical microscope and gentle suction a small cortical area was resected. A tumor piece was placed in the resection cavity and the skin was closed using surgical staples. All animals were treated in accordance with the policies and guidelines of the Johns Hopkins University Animal Care and Use Committee.

2.4. D-Cy5 administration for quantification and immunofluorescence

Animals were injected in tail vein with a 3 mg/300 μL dendrimer conjugated-Cy5 (D-Cy5) solution. For imaging of dendrimer and dextran distribution, 3 animals were co-injected with a 0.9% NaCl solution of 2 mg D-Cy5 and 2 mg dextran-FITC in 300 μL.

To study the dynamics of dendrimer accumulation in the tumor brain, D-Cy5 was injected into 27 tumor inoculated rats when the average tumor size was 6 mm in diameter and then animals were sacrificed at fixed time points (15 min, 1 h, 4 h, 8 h, 24 h, and 48 h). Magnetic resonance imaging was used to measure intracranial tumor size. Blood was drawn through cardiac puncture and immediately centrifuged to collect plasma. Brains were harvested and flash frozen on dry ice for fluorescence spectroscopy based quantification or placed in 4% formalin solution for immunofluorescence.

To study the dendrimer cell uptake, D-Cy5 injection was performed in 3 tumor inoculated rats and 3 healthy rats, and animals were sacrificed 24 h after the injection. Brains were harvested and placed in 4% formalin for immunofluorescence study.

To study the pharmacokinetics and biodistribution of dendrimer in plasma and systemic organs D-Cy5 was injected into 15 tumor-inoculated rats which were placed in metabolic cages for urine collection and animals were subsequently euthanized at fixed time points (15 min, 1 h, 4 h, 8 h, 24 h, and 48 h). Organs were harvested and flash frozen on dry ice for fluorescence spectroscopy-based quantification or placed in 4% formalin for immunofluorescence.

2.5. Fluorescence spectroscopy

Fluorescence-based quantification of D-Cy5 conjugates followed our previously published protocol [27]. Briefly, 100–150 mg of frozen tissue was homogenized in 1 mL of methanol using a homogenizer (TissueLyser LT, Giagen) in 2 mL DNA LoBind Eppendorf tubes and subsequently sonicated. Suspensions were diluted to 100 mg/mL and centrifuged at 15,000 rpm for 15 min at 4 °C. The resulting supernatants were subjected to fluorescence spectroscopy. Importantly, prior studies showed that D-Cy5 was stable in plasma, and could be recovered from the tissue intact, without appreciable release of the conjugated Cy5 [27].

For brain tissue, precise dissection of the tumor was performed and the peritumoral area was defined as up to 1 mm away from the tumor dissection plane. In the contralateral hemisphere 100 mg of the caudate/putamen with the surrounding white matter area was dissected and used for analysis. For plasma and urine samples, a sample of 100 μL of plasma and urine was mixed with 900 μL of phosphate buffer (0.1 M) and analyzed by fluorescence spectroscopy.

Fluorescence spectra of D-Cy5 conjugates and that obtained from tissue extracts were recorded using a Shimadzu RF-5301 Spectrofluorophotometer (Kyoto, Japan). D-Cy5 calibration curves were constructed, following every experiment, under different slit widths using the maximum emission wavelength of 662 nm after recording spectra from 650 nm to 720 nm with excitation wavelength of 645 nm. The D-Cy5 concentration was measured in methanol or phosphate buffer (0.1 M) in solutions ranging from 1 ng/mL to 100 μg/mL. The slit width was chosen based on the observed fluorescence level of different sample sets. For biological samples with low levels of D-Cy5 (i.e. brain, lung, heart), the excitation and emission slit width was set at 10; for biological samples with high levels of D-Cy5, (i.e. urine and kidney) excitation and emission slit width were set at 3. For the remaining biological samples, excitation slit width of 5 and emission slit width of 10 were used. All calibration curves exhibited linearity with $R^2 \sim 0.99$. Fluorescence registered from tissue of non D-Cy5 injected healthy and tumor inoculated rats was subtracted from the values observed from samples of D-Cy5 injected tissue in order to account for tissue autofluorescence.

Concentration of D-Cy5 conjugate in the brain was expressed in μg per g of tissue. The concentration of D-Cy5 conjugate in the other organs was expressed in percentage (%) of injected dose per gram of tissue or % of injected dose per organ. Concentrations of the D-Cy5 conjugate in urine and blood were expressed in % of injected dose per mL or % of injected dose in total amount of urine or plasma. Total plasma concentration was calculated based on the weight of the animal. The brain and plasma quantification data were analyzed to calculate the area under curve (AUC) and the brain to serum ratio.

The permeation constant (Kin) and the initial volume of distribution (Vi) were calculated in the brain tumor [29]. The brain to serum ratio and the area under the curve of the serum (AUC(serum) (t)) to serum concentration (Serum(t)) were calculated for each time point and linear regression analysis was performed in order to get the Kin and Vi based the following equation:

$$\frac{Brain(t)}{Serum(t)} = K_{in}\frac{AUCserum(t)}{Serum(t)} + V_i$$

For all three regions in the brain, the multiple time-point regression analysis showed good linearity with R2 equal to 0.98, 0.99, and 0.96 for the contralateral hemisphere, the peritumoral, and the tumor region, respectively.

2.6. Immunofluorescence

Freshly harvested tissues were fixed in 4% formalin for 24 h, followed by a gradient of sucrose solutions before cryosection. Tissues were then sectioned axially into 30 μm-thick slices using a Leica CM 1905 cryostat. Slices were stained with DAPI (nuclei), rabbit anti-Iba1 antibody for microglia/macrophages, and goat anti-rabbit 595 secondary antibody. Some slices were stained with isolectin for endothelial cell staining. Slices were then imaged using a confocal LSM 710 microscope (Carl Zeiss; Hertfordshire, UK) under 5X, 20X, 40X and 63X magnifications. For each slice of tumor-inoculated brains, images were acquired for the tumor, tumor border and contralateral hemisphere. For control (non-tumor) brains, 1–3 representative images were acquired. Settings were optimized to avoid background fluorescence based on non-injected control rat brains. Laser power, pinhole, gain, offset and digital gain were selected separately for each magnification and kept constant throughout the entire study.

2.7. Software

For image processing ZEN 2011 software was used, any adjustments in brightness and contrast were kept constant throughout the same magnification images. No adjustments were done on the Cy5 channel. Imaris software was used for cell counting, co-localization and microglia surface to volume ratio measurements. Microsoft Excel 2010 and KaleidaGraph 4.0 were used for all calculations, curve fitting and figure plotting related to the pharmacokinetic study.

2.8. Cell count and co-localization

For microglia/macrophage cell count, 20 × 13 × 13 tile scan images were analyzed and 3–5 slices were analyzed per region. The function 'spots' was used to identify Iba1+ microglia/macrophages. A diameter threshold of 4.15 μm was set to eliminate the objects smaller than microglia cells and an intensity threshold of 26.801 based on 'Quality' analysis was set to eliminate the background signal [30].

To study co-localization 40X, 4 × 4 tile scan images were used and 3–5 slides were analyzed per region. The function 'spots' was used to identify DAPI+ nuclei, Iba1+ microglia/macrophages and D-Cy5+ cells. For cells with D-Cy5 uptake, the spots with D-Cy5 and DAPI co-localization were counted; for microglia cells with D-Cy5 uptake, the spots with DAPI, anti-Iba1 and D-Cy5 co-localization were counted. Estimated diameters were applied to eliminate the spots with size smaller than cells, and signal thresholds were applied based on 'Quality' analysis. The function co-localize spots was used by counting the spots where D-Cy5 signal and cell signal are within 10 μm next to each other [30].

For surface to volume ratio analysis of the microglia cells, 3D representation of microglia morphology was acquired in confocal microscope using 40X magnification, with 3 × 3 tile scan, extending 10 μm in the z direction in z-stack. The function 'surfaces' was used and the individual Iba1+ microglia/macrophages were analyzed for surface and volume of each cell. Tumor area, ipsilateral (non-tumor area), contralateral area, and non-tumor brains were analyzed; approximately 150 cells were included for each region. The threshold settings were based on the diameter of cells [31].

2.9. Statistical analysis

Statistical analysis of data was carried out by student's t-test and one-way ANOVA followed by Games–Howell tests using SPSS 18.0 (IBM, Inc.), as needed. Differences were considered statistically significant at $p < 0.05$.

3. Results

3.1. Pharmacokinetics of systemically delivered dendrimer in brain tumor

Based on confocal microscopy, dendrimer-Cy5 conjugates (D-Cy5) rapidly accumulated throughout a 6 mm tumor, as early as 15 min after systemic administration. In the 'healthy' contralateral hemisphere, dendrimers outlined the blood vessels, and were not observed in the parenchyma (Fig. 1A,D). Fifteen minutes after systemic administration, the dendrimers were dispersed throughout the entire intracranial tumor parenchyma. This distribution was not influenced by the heterogeneity in the tumor parenchyma (Fig. 1B). There was no appreciable cellular uptake at this time point. At 4 h post systemic dendrimer administration, the extracellular distribution in the tumor region had decreased, which was accompanied by an increased uptake by Iba1+ inflammatory cells (Fig. 1C). The contralateral hemisphere showed relatively minimal D-Cy5 fluorescence at all-time points (Fig. 1D,E).

In order to assess the kinetics of dendrimer accumulation in the brain, we used a recently developed fluorescence-based quantification method for D-Cy5. The use of the near IR Cy5 wavelength overcomes the tissue autofluorescence challenges [27]. The high sensitivity of this method (0.1 ng/g of tissue) allowed us to detect dendrimer accumulation at specific anatomic locations. In accordance with our confocal microscopy results, dendrimers rapidly accumulated in the tumor and peritumoral area within 15 min, with a peak concentration occurring at 8 h (Fig. 2A). Dendrimers gradually cleared from the tumor at a rate of ~0.01 μg/g/hr, and from the peritumoral area at a rate of ~0.007 μg/g/hr, reaching a concentration of 0.2 μg/g of tissue 48 h after initial systemic injection (Fig. 2A). In the contralateral hemisphere, the dendrimer accumulation also peaked at 8 h, at a concentration ~ 8-fold lower than that found in the tumor area. At 24 h, traces of dendrimer (0.03 μg/g) could be detected in the contralateral hemisphere and a ~14 fold higher accumulation in the tumor was observed (Fig. 2A). At 48 h the area under the curve (AUC) was 10 times higher in the tumor area in comparison to the contralateral hemisphere, indicating significantly higher ($p < 0.05$) overall exposure of the dendrimer to the tumor (Fig. 2B). The high and selective retention of dendrimer in the tumor and peritumoral area was visualized in a low magnification image of the tumor stained for astrocytes 24 h following the administration of dendrimer (Fig. 2C).

The vasculature and the amount of BBTB disruption have been demonstrated to differ significantly between the tumor core and a tumor border, which may play a significant role in drug accumulation [32]. In Fig. 3A we stained for blood vessel endothelial cells in order to examine the difference in vasculature and, therefore, perfusion between the tumor and the peritumoral area. As expected, the peritumoral area and the tumor border showed dramatically denser vasculature than the tumor core. However, the dendrimer distribution appeared to be uniform in the tumor.

To further understand the kinetics of dendrimer penetration in the tumor we calculated the permeation constant (Kin) and the initial volume of distribution (Vi) in the tumor, peritumoral area and contralateral hemisphere (Fig. 3B). Kin describes the influx of dendrimer from the blood to the brain, and was 10 fold higher in the tumor and peritumoral area in comparison to the contralateral hemisphere (Fig. 3C), indicating the increased penetration of dendrimers and increased permeability and perfusion of the tumor tissue. Vi represents the volume of the brain compartments in rapid equilibrium with plasma, differed significantly between the tumor and the peritumoral area (Fig. 3C) indicating a larger volume of rapid equilibration in the tumor core. In tumor xenografts the hypoxic tumor core has increased vascular permeability in comparison to the tumor border [33] and in glioblastoma specifically a distinct difference in the morphology of the BBTB between the tumor core and the peritumoral area has been shown, which may contribute to the rapid distribution in the tumor core as opposed to the peritumoral area [32].

3.2. Time dependent distribution of D-Cy5 in the brain tumor

To study the dendrimer distribution in the tumor and peritumoral area, we co-injected D-Cy5 with linear dextran-FITC (70 kDa, ~6.5 nm radius) which has approximately twice the size of dendrimer. The tumor was clearly identified based on the increased density of DAPI+ nuclei (Fig. 4A). At each time point, the dendrimer distributed homogeneously throughout the whole tumor region (Fig. 4B). In comparison, signal from dextran-FITC was only observed around the tumor border and not in the tumor core, even though the laser power and gain settings were maximized to detect

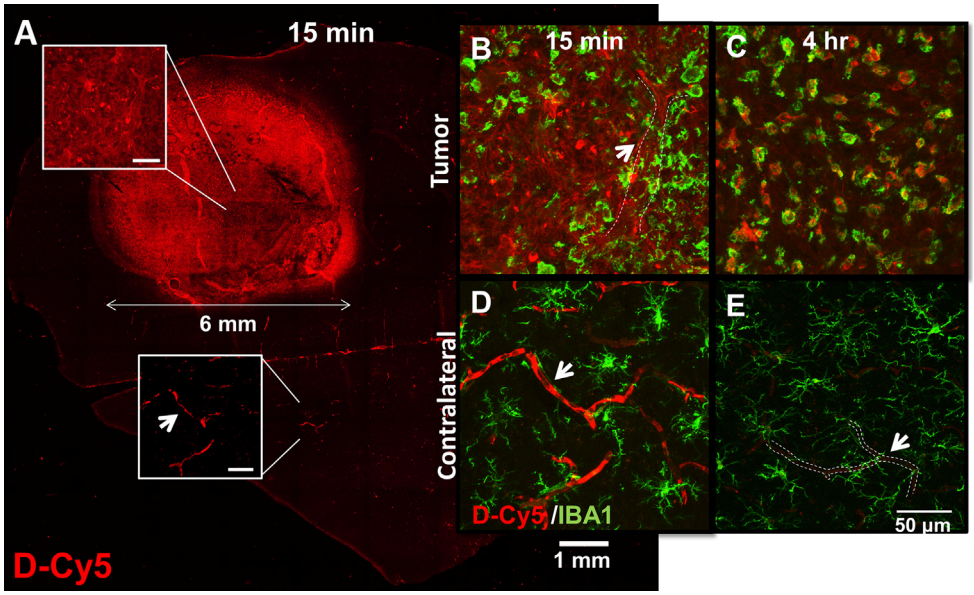

Fig. 1. Confocal microscopy images of tumor-inoculated rodent brain following systemic administration of D-Cy5. The dendrimer-Cy5 conjugate distributes throughout the solid tumor, in TAMs. (A) Low magnification image of tumor inoculated brain, 15 min following systemic administration of D-Cy5. Scale bar: 1 mm. Inset images indicate the homogeneous distribution of D-Cy5 in the tumor and the restriction of dendrimer in the blood vessel lumen of the contralateral hemisphere. Scale bar: 50 μm (B) High magnification images of the tumor and contralateral hemisphere 15 min and 4 h post I.V. administration. Red: D-Cy5; Green: Iba1+ microglia/macrophages. Scale bar: 50 μm. Arrow and dashed line delineate blood vessels. (For interpretation of the references to color in this figure legend, the reader is referred to the web version of this article.)

the background signal in the FITC channel (Fig. 4C). Higher magnification images showed that D-Cy5 rapidly distributed and delineated the ECM leading to a reticular pattern of distribution and gradual accumulation in the cells (Fig. 4D). On the contrary, dextran-FITC showed limited distribution throughout the ECM, but high signal could be seen within the blood vessel lumen 15 min after injection. At later time points, limited amounts of dextran-FITC were retained in the tissue presumably due to low cellular uptake (Fig. 4E).

3.3. Characterization of tumor associated microglia/macrophages and cellular uptake of dendrimer

Gliomas produce chemo-attractants and growth factors that promote recruitment and proliferation of microglia/macrophages [34,35]. In human glioblastoma up to 30% of cells can be tumor associated macrophages [36]. We characterized the microglial distribution in different anatomic locations of the 9L tumor model, which suggested that the concentration of TAM in this tumor model is similar to that observed in human glioblastoma. The microglia/macrophage population per mm^2 was 9-fold higher within the tumor as compared to the contralateral hemisphere and 2.5-fold higher in healthy brain tissue of the ipsilateral hemisphere as compared to the contralateral hemisphere (Fig. 5A).

TAM are reprogrammed in the tumor microenvironment leading to an alternate immunosuppressive M2 phenotype [34]. However, a number of studies have suggested sustained phagocytic activity of TAM in glioma. The phagocytic activity of TAM has been suggested to play a key role in nanoparticle uptake [25] and [26]. When microglia/macrophages change from a resting to an activated form, their morphology is modified from ramified to amoeboid indicative of their increased phagocytic activity [37]. In order to assess the morphology of TAM in the 9L tumor model, we characterized the cell surface area to cell volume ratio (StoV ratio) of the immune cell population (Iba1+) in different anatomical locations [38]. The StoV ratio is considered a 'measure' of microglial activation [31]. Our results suggest that, indeed, the microglia/macrophages within the tumor and surrounding the tumor had a significantly ($p < 0.001$) lower StoV ratio in comparison to the immune cells in the contralateral hemisphere, and in a healthy brain. The mean StoV ratio for tumor associated microglia was lower than 1, indicative of their amoeboid state and phagocytic activity (Fig. 5B).

We then quantified the localization of D-Cy5 in the Iba1+ microglia/macrophages cells. At 24 h post systemic administration dendrimers localized in the Iba1+. In fact, TAM Iba1+ microglia/macrophages were calculated to comprise 38% of the total tumor cell population (Fig. 6A). Co-localization indicated that approximately half of the TAM population took up dendrimers and that the total population of D-Cy5+ cells did not differ quantitatively from the population of dendrimer-positive Iba1+ microglia/macrophages. Therefore, dendrimers were taken up almost exclusively by tumor associated macrophages within the tumor tissue (Fig. 6A), while other cells within the tumor region didn't have measurable dendrimer uptake. Representative images of cellular uptake of dendrimer in the tumor are demonstrated in Fig. 6B and C. Interestingly, in the tumor border (indicated as 1 mm from the tumor edge based on DAPI stain) the D-Cy5+ microglia/macrophages were substantially reduced, reflecting the difference in the biological processes between the tumor core and the tumor border. Dendrimer was not observed in the ipsilateral non-tumor region or in the contralateral hemisphere (Fig. 6D–F).

3.4. Systemic biodistribution of D-Cy5

After 24 h from systemic administration, fluorescence-quantification of extracted D-Cy5, suggested that 56% of the dendrimer was excreted through the urine, while 32% remained in the kidneys. This correlates well with the low serum levels (0.66%, Fig. 7A) at this time point. After 24 h from systemic administration, only 2.5% of the dendrimers were accumulated in other major organs. 1.5% of these dendrimers were retained in the liver and spleen representing the elimination by the reticuloendothelial system (RES). Trace amounts accumulated in the brain, lung and heart.

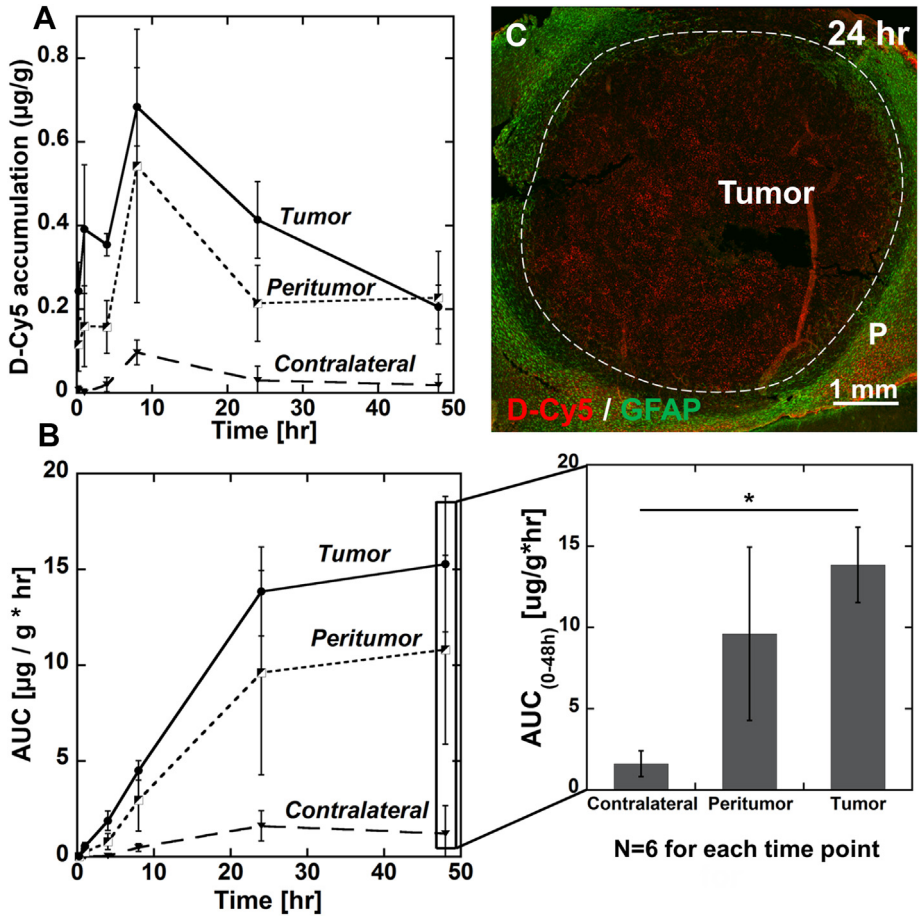

Fig. 2. D-Cy5 pharmacokinetics in the brain (tumor, peritumor and contralateral hemisphere) of a rodent 9L gliosarcoma model. (A) D-Cy5 concentration in brain areas 15 min, 1 h, 4 h, 8 h, 24 h and 48 h following systemic administration. The accumulation is expressed as μg of D-Cy5 per g of tissue. Data represents mean ± standard error of the mean (SEM) (B) Exposure of respective brain areas to D-Cy5 following systemic administration as expressed by the AUC of D-Cy5 concentration at different time points. The AUC at 48 h demonstrates the statistically significant difference in dendrimer accumulation between the tumor and the contralateral hemisphere ($p < 0.05$). (C) Fluorescence-microscopy image demonstrating vascular density and D-Cy5 accumulation in brain tumor 24 h post I.V. administration. Red: D-Cy5; Green: GFAP (physiologic astrocytes). T: Tumor P: Peritumoral area C: Contralateral area; Scale bar: 1 mm. (For interpretation of the references to color in this figure legend, the reader is referred to the web version of this article.)

To better understand the kinetics, dendrimer concentration in the serum and major organs was measured over time (Fig. 7B). The kidney had an increasing accumulation at all chosen time points up to 24 h. At 48 h the amount of dendrimer in the kidneys began to decrease. Dendrimer cleared rapidly from plasma, with only 1% of the injected dose detected at 8 h after systemic administration (Fig. 7C). This amount is still significantly higher than the dendrimer accumulation in the brain, thus correlating well with the

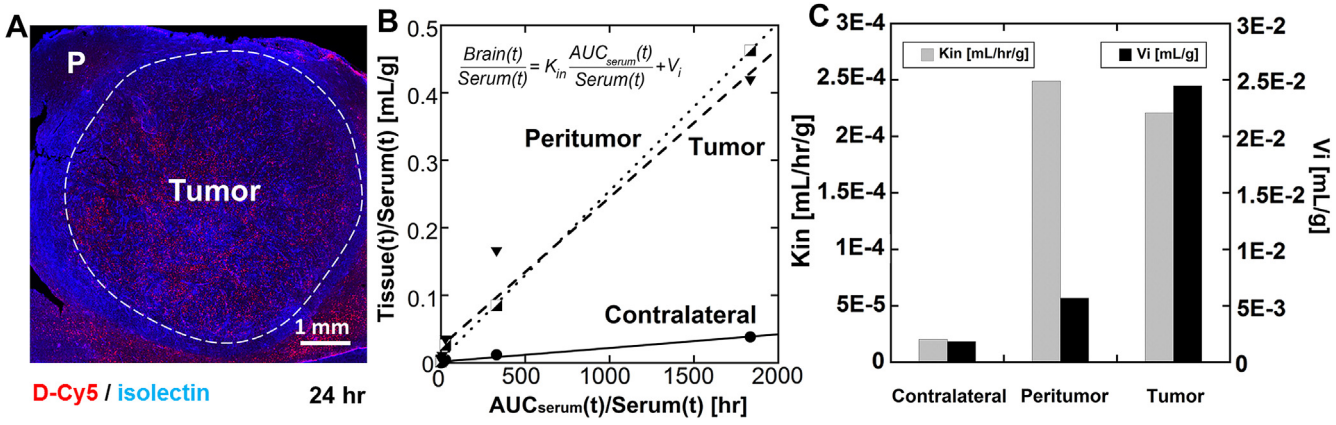

Fig. 3. Calculation of permeation constant (K_{in}) and initial volume of distribution (V_i) in tumor, peritumoral area and contralateral hemisphere based on brain pharmacokinetics data (Fig. 2). (A) Fluorescence-microscopy image demonstrating vascular density and D-Cy5 accumulation in brain tumor 24 h post I.V. administration. T: Tumor; P: Peritumoral area; Scale bar: 1 mm. (B) Linear curve fitting based on brain quantification data. The R2 for contralateral, peritumor and tumor are 0.98, 0.99 and 0.96, respectively. (C) K_{in} and V_i at respective brain areas.

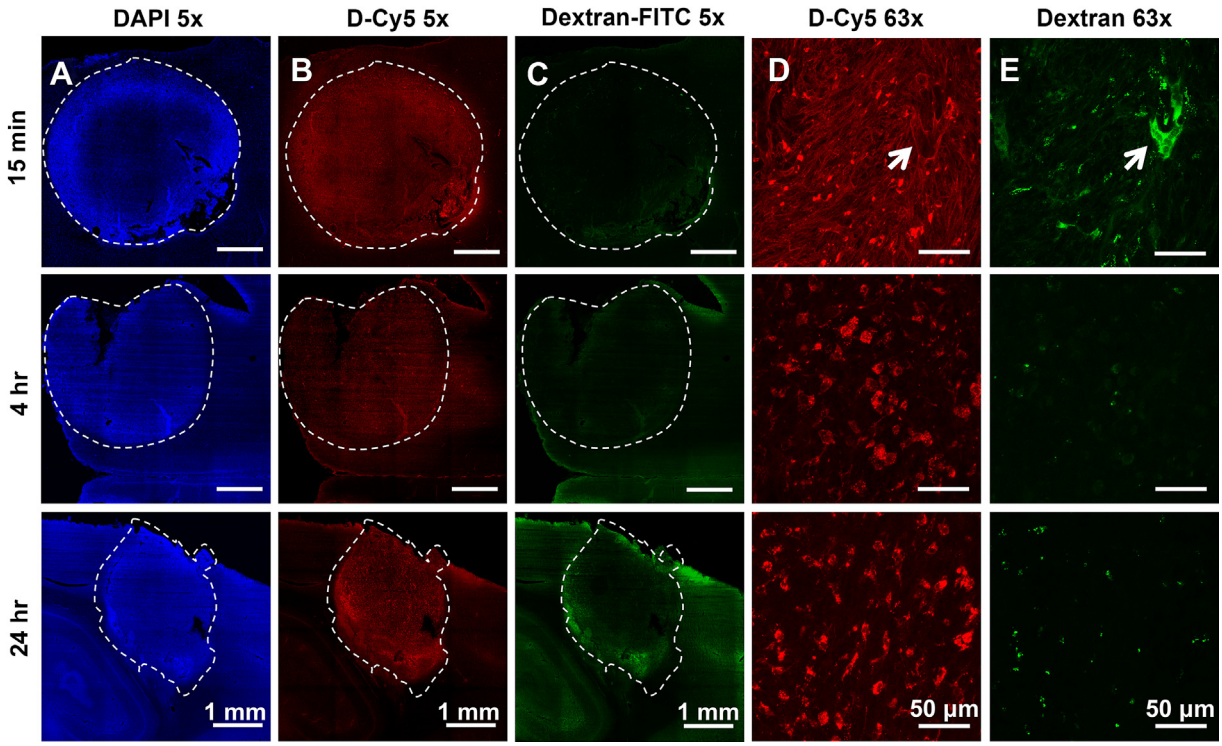

Fig. 4. Confocal microscopy imaging of 9L gliosarcoma rodent brains following systemic co-administration of D-Cy5 and 70 kDa Dextran-FITC. (A–C) Low magnification and (D, E) high magnification images of D-Cy5 and Dextran-FITC distribution in the tumor area. Blue: DAPI staining of nuclei indicative of the tumor region; Red: D-Cy5; Green: Dextran-FITC. Scale bar: 1 mm (Column A–C) and 50 μm (Column D and E). White arrow indicates a blood vessel based on DAPI staining (not shown). (For interpretation of the references to color in this figure legend, the reader is referred to the web version of this article.)

increased accumulation of dendrimer within the tumor 8 h post injection.

3.5. Renal accumulation and distribution

The high concentration of dendrimer in the renal system led us to study the distribution in the kidney in order to assess the sites of accumulation. Based on fluorescence microscopy, the dendrimer accumulated in the renal cortex (Fig. S1, panel A). Dendrimer co-localized with anti-GFAP antibody which stained the peritubular fibroblasts (Fig. S1, panel B). No presence of dendrimer was observed in the glomeruli. There was no significant difference in terms of the clearance through the kidneys among healthy and tumor-bearing rats.

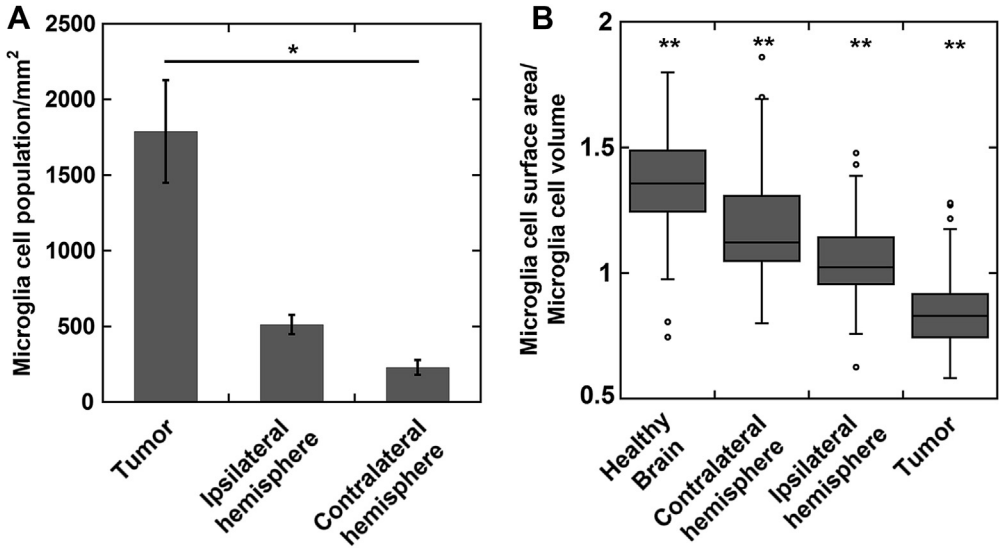

Fig. 5. Characterization of microglia cells (population and activation status) in a 9L gliosarcoma inoculated rodent brain using Imaris software. (A) Image-based cell count of the Iba1+ microglia/macrophages population per mm2 area in the tumor, ipsilateral hemisphere and contralateral hemisphere; *$p < 0.05$ (B) Image-based measurement of microglia cell surface to volume ratio as an indication of activation status and phagocytic activity of microglia/macrophages in healthy brain, contralateral hemisphere and ipsilateral hemisphere of a tumor inoculated brain and tumor tissue. **$p < 0.001$; Statistical analysis is based on 3–5 different slices.

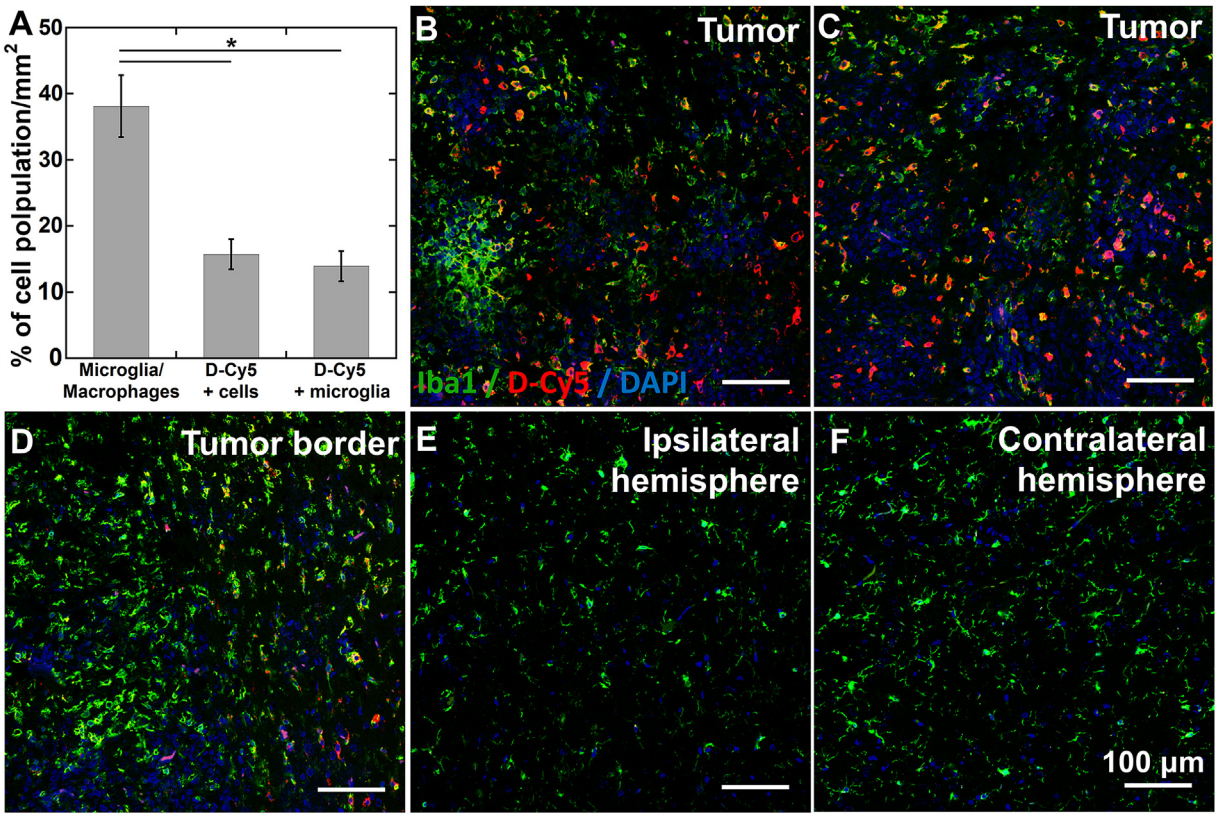

Fig. 6. D-Cy5 cellular uptake analysis 24 h following systemic administration. (A) Image based measurement of Iba-1+ cells, D-Cy5 co-localization with Iba1+ TAM, and D-Cy5 co-localization with DAPI + cells. Results are expressed as percent of the total DAPI + cell population. *$p < 0.05$; There is no statistical significance between microglia uptake and cell uptake. (B–F) High magnification (40X) fluorescence confocal imaging of different anatomic locations of a 9L gliosarcoma inoculated brain. Green: Iba1+ microglia/macrophages, Red: D-Cy5, Blue: DAPI. Scale bar: 100 μm. Statistical analysis is based on 3–5 different slices. (For interpretation of the references to color in this figure legend, the reader is referred to the web version of this article.)

4. Discussion

In this study, we investigated hydroxyl-terminated, generation-4 PAMAM dendrimers as potential drug delivery vehicles for the delivery of therapeutics to brain tumors. The systemically delivered dendrimers accumulated and were selectively retained in intracranial tumor tissue. Moreover, they rapidly and 'homogeneously' distributed throughout the entire 6 mm solid tumor and peritumoral area, followed by a gradual accumulation in TAM. Apart from the retention in tumor associated

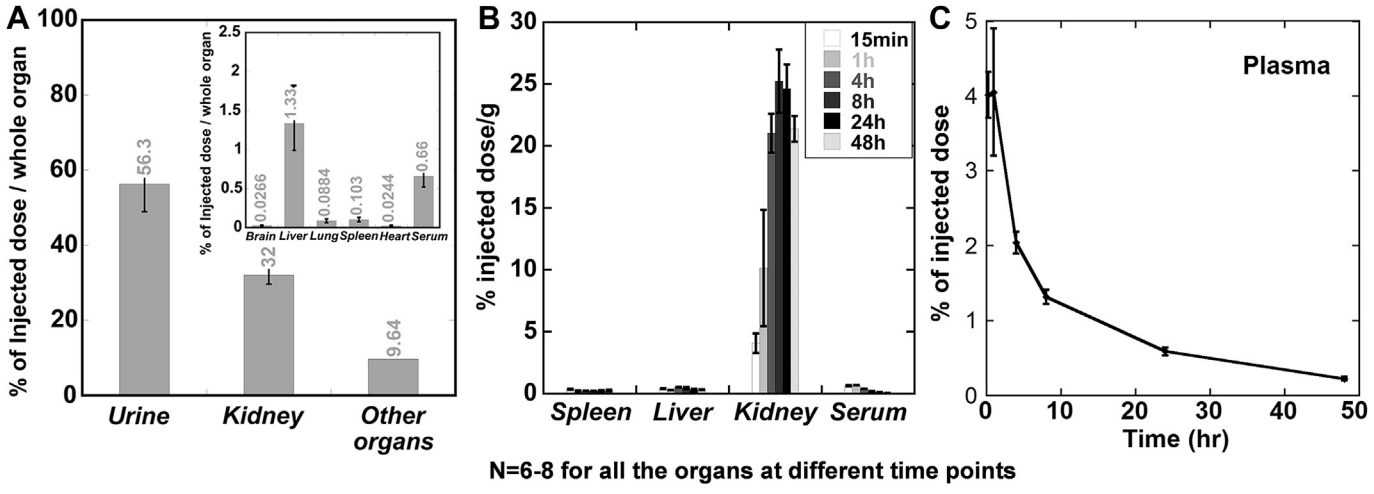

Fig. 7. Systemic biodistribution and pharmacokinetics of D-Cy5. (A) Fluorescence-based quantification of D-Cy5 in serum and urine and major organs (brain, liver, lung, spleen, heart, and kidney) of 9L gliosarcoma rodent model 24 h following D-Cy5 administration. The biodistribution is expressed in percent of injected dose per organ; (inserted panel): D-Cy5 accumulation in kidney, urine and other organs. (B) Time dependent concentration of D-Cy5 in spleen, liver, kidney and serum. Concentration is expressed as percent of injected dose per g of tissue. (C) Fluorescence-based quantification of the plasma pharmacokinetics of D-Cy5.

neuroinflammatory cells, dendrimers exhibited a pharmacokinetic profile similar to that shown in healthy animals with a short circulation half-life and rapid renal excretion [27,39]. This suggests that these dendrimers may enable selective therapeutic delivery to the brain tumor with rapid clearance from off-target organs.

Small molecule therapeutics may pass the impaired BBTB, but are rapidly cleared from the tumor tissue and also distribute in other organs, resulting in limited effect on the tumor cells and side effects [40–42]. Various nanoparticle systems have demonstrated relatively selective and sustained accumulation in extracranial tumors and allowed for controlled release of chemotherapeutics [6,8,43,44]. However, the size limitation of the BBTB capillary fenestrations and the hindered nanoparticle motion in the heterogeneous brain tumor parenchyma does not allow for high accumulation and homogeneous distribution in brain tumors [10,45,46]. We show that dendrimers accumulate selectively and rapidly in an intracranial tumor and are retained in the tumor for at least 48 h. Of note, at 4 h post injection, dendrimer accumulation is approximately 10 fold higher in the tumor region compare with the small molecule drug doxorubicin [47]. Also, for dendrimers, the AUC(0–24 h) in the tumor is 8.5 fold higher than that in the contralateral hemisphere, demonstrating improved 'intrinsic' targeting in comparison to other non-targeted nanoparticle systems and is comparable to actively targeted magnetic nanoparticles [48]. Moreover, high concentrations of dendrimer were observed in the peritumoral area. The high frequency of glioblastoma recurrence is attributed to high tumor infiltration as well as individual cells surviving the initial aggressive treatment. Therefore, achieving high retention in the peritumoral area is important in the design of an effective therapeutic vehicle [49]. Interestingly, in the peritumoral area, the accumulation rate and the initial volume of distribution were lower than those in the tumor core. This may be attributed to the increase vascular permeability and BBTB leakage of the hypoxic tumor core in comparison to the relatively intact BBTB in the peritumoral area [32].

Recent studies have maintained that efficient distribution of nanoparticles throughout the solid tumor tissue is nearly mandatory for efficacy [50–53]. The highly heterogeneous vasculature of glioblastoma requires the particles to escape the perivascular spaces and move a distance of at least 80 nm in order to cover the intervascular spaces [50,54]. Perrault et al. have demonstrated that in a subcutaneous tumor model, PEGylated gold nanoparticles larger than 20 nm get entrapped in the perivascular spaces [51]. We demonstrate that after dendrimers pass through the BBTB, they rapidly distribute through the ECM within 15 min and cover the entire tumor. This observation can most likely be attributed to the small size and near neutral surface charge of the dendrimers that allow them to escape the perivascular spaces and penetrate the tumor tissue.

Our lab has previously reported that non-targeted dendrimers localized in activated microglia in the periventricular area of rabbit neonates with neuroinflammation following intravenous administration [17]. This selective cellular uptake allowed for therapeutic effect, with significant motor function improvement, following delivery of dendrimer-N-acetylcysteine conjugates [17]. Of note, this was achieved in spite of only 0.06% of injected dose per gram of tissue at injured region, at 24 hr post injection, thus, underlining the importance of cell-specific targeting, rather than overall accumulation, for improved therapeutic outcome. In the present study we found that 24 h after administration, dendrimers almost completely localized in TAM and that approximately 50% of the TAM population had taken up dendrimers. The dendrimers were not seen in 'non-activated'/quiescent microglia/macrophages. The high concentration of phagocytic cells in this tumor in combination with the remarkably high accumulation of dendrimers in TAM may contribute to their retention in glioblastoma. The mechanism of nanoparticle accumulation in TAM has previously been investigated using cyclodextrin-based particles and carbon nanotubes. It is possible that both invading macrophage/monocytes take up nanoparticles in the circulation but also that TAM within glioma take up nanoparticles after they distribute in the tumor parenchyma [25]. However, the rapid distribution of dendrimer in the tumor, the rapid elimination from the circulation and the low accumulation in the reticuloendothelial system, suggest that the dendrimers localize more through the latter mechanism. To clarify, the TAM uptake shown by dendrimers is specific to activated cells in the tumor, different from the typical systemic macrophage uptake/clearance of larger nanoparticles. Neuroinflammation and TAM have important growth promoting and pro-invasive effects in brain tumors. TAM is subjected to reprogramming in the tumor microenvironment, leading to an alternate immunosuppressive tumorigenic M2 phenotype [34]. Topically administered immunomodulatory which block the M2-related phenotype of TAM are being investigated for the treatment of glioblastoma [19,20]. Dendrimer-specific accumulation in TAM with low retention in the reticuloendothelial system and rapid clearance from the circulation, suggest that these systematically delivered dendrimers are promising candidates for the delivery of anti-glioma therapies targeting TAM.

As previously reported [27,39], dendrimers were rapidly cleared through renal excretion. This is expected as the renal filtration cut off size is approximately 5.5 nm [55]. After 24 h from systemic injection of the dendrimers, more than half of the injected amount was excreted in the urine and 32% of the injected dose was in the kidneys. The increased accumulation of dendrimers in the proximal convoluted tubules is in agreement with previous reports [27,56]. No dendrimer accumulation was observed in the glomeruli or the interstitial space. Given the selective uptake in the tubule epithelial cells and the various mechanisms of reabsorption occurring in the proximal tubule [57], an active reabsorption mechanism may be responsible for this distribution pattern. The ability of PAMAM dendrimer to target TAMs in brain tumors from systemic administration may bring new opportunities for targeted tumor immunotherapies, with reduced side effect [58].

5. Conclusion

Systemically delivered hydroxyl, generation-4 PAMAM dendrimers rapidly accumulate (~fifteen minutes) and are selectively retained in an in vivo intracranial brain tumor model. The dendrimers homogeneously distribute throughout the entire 6 mm solid tumor and peritumoral area and gradually accumulate in TAM. This homogeneous distribution is retained for at least 48 h indicating that the dendrimers used in this study may be effective vehicles for delivery of chemotherapeutics. Also, the intrinsic targeting of neuroinflammatory cells which play a critical role in the aggressive nature of glioblastoma may allow for enhanced delivery of immunomodulatory molecules to TAM. This study of the pharmacokinetics and biodistribution of dendrimers in an intracranial brain tumor model provides insights for the design and engineering of systemically-delivered dendrimer-drug conjugates for improved efficacy, and reduced side effects for brain tumors.

Acknowledgments

We thank the Wilmer Core Module for Microscopy and Imaging for allowing us to use LSM710 confocal microscopy. We also thank Dr. G. Lutty's Lab for the use of Imaris software. We thank Dr. E.

Nance for manuscript review and valuable suggestions. No funding source contributed to this study.

Appendix A. Supplementary data

Supplementary data related to this article can be found at http://dx.doi.org/10.1016/j.biomaterials.2015.02.053

References

[1] Schwartzbaum JA, Fisher JL, Aldape KD, Wrensch M. Epidemiology and molecular pathology of glioma. Nat Clin Pract Neurol 2006;2:494–503. quiz 1 p following 16.
[2] Bregy A, Shah AH, Diaz MV, Pierce HE, Ames PL, Diaz D, et al. The role of Gliadel wafers in the treatment of high-grade gliomas. Expert Rev Anticancer Ther 2013;13:1453–61.
[3] Jain RK, Stylianopoulos T. Delivering nanomedicine to solid tumors. Nat Rev Clin Oncol 2010;7:653–64.
[4] Rittierodt M, Harada K. Repetitive doxorubicin treatment of glioblastoma enhances the PGP expression–a special role for endothelial cells. Exp Toxicologic Pathol: Off J Gesellschaft fur Toxikologische Pathologie 2003;55:39–44.
[5] Heath JR, Davis ME. Nanotechnology and cancer. Annu Rev Med 2008;59:251–65.
[6] Cabral H, Matsumoto Y, Mizuno K, Chen Q, Murakami M, Kimura M, et al. Accumulation of sub-100 nm polymeric micelles in poorly permeable tumours depends on size. Nat Nanotechnol 2011;6:815–23.
[7] Wu W, Driessen W, Jiang XQ. Oligo(ethylene glycol)-based thermosensitive dendrimers and their tumor accumulation and penetration. J Am Chem Soc 2014;136:3145–55.
[8] Tang L, Gabrielson NP, Uckun FM, Fan TM, Cheng JJ. Size-dependent tumor penetration and in vivo efficacy of monodisperse drug-silica nanoconjugates. Mol Pharm 2013;10:883–92.
[9] Schadlich A, Caysa H, Mueller T, Tenambergen F, Rose C, Gopferich A, et al. Tumor accumulation of NIR fluorescent PEG PLA nanoparticles: impact of particle size and human xenograft tumor model. ACS Nano 2011;5:8710–20.
[10] Tzeng SY, Green JJ. Therapeutic nanomedicine for brain cancer. Ther Deliv 2013;4:687–704.
[11] Sarin H, Kanevsky AS, Wu H, Brimacombe KR, Fung SH, Sousa AA, et al. Effective transvascular delivery of nanoparticles across the blood-brain tumor barrier into malignant glioma cells. J Transl Med 2008;6:80.
[12] Sarin H. Recent progress towards development of effective systemic chemotherapy for the treatment of malignant brain tumors. J Transl Med 2009;7:77.
[13] Sarin H. Effective transvascular delivery of chemotherapy into cancer cells with imageable nanoparticles in the 7 – 10 nanometer size range. In: Slevin M, editor. current advances in the medical application of nanotechnology. Bentham Science Publishers Ltd; 2012. p. 10–24.
[14] Hobbs SK, Monsky WL, Yuan F, Roberts WG, Griffith L, Torchilin VP, et al. Regulation of transport pathways in tumor vessels: role of tumor type and microenvironment. Proc Natl Acad Sci U S A 1998;95:4607–12.
[15] Mishra MK, Beaty CA, Lesniak WG, Kambhampati SR, Zhang F, Wilson MA, et al. Dendrimer brain uptake and targeted therapy for brain injury in a large animal model of hypothermic circulatory arrest. ACS Nano 2014;8:2134–47.
[16] Sykova E, Nicholson C. Diffusion in brain extracellular space. Physiol Rev 2008;88:1277–340.
[17] Kannan S, Dai H, Navath RS, Balakrishnan B, Jyoti A, Janisse J, et al. Dendrimer-based postnatal therapy for neuroinflammation and cerebral palsy in a rabbit model. Sci Transl Med 2012;4. 130ra46.
[18] da Fonseca AC, Badie B. Microglia and macrophages in malignant gliomas: recent discoveries and implications for promising therapies. Clin Dev Immunol 2013;2013:264124.
[19] El Andaloussi A, Sonabend AM, Han Y, Lesniak MS. Stimulation of TLR9 with CpG ODN enhances apoptosis of glioma and prolongs the survival of mice with experimental brain tumors. Glia 2006;54:526–35.
[20] Hussain SF, Kong LY, Jordan J, Conrad C, Madden T, Fokt I, et al. A novel small molecule inhibitor of signal transducers and activators of transcription 3 reverses immune tolerance in malignant glioma patients. Cancer Res 2007;67:9630–6.
[21] Gabrusiewicz K, Ellert-Miklaszewska A, Lipko M, Sielska M, Frankowska M, Kaminska B. Characteristics of the alternative phenotype of microglia/macrophages and its modulation in experimental gliomas. PloS One 2011;6.e23902.
[22] Markovic DS, Vinnakota K, van Rooijen N, Kiwit J, Synowitz M, Glass R, et al. Minocycline reduces glioma expansion and invasion by attenuating microglial MT1-MMP expression. Brain, Behav Immun 2011;25:624–8.
[23] Dreaden EC, Mwakwari SC, Austin LA, Kieffer MJ, Oyelere AK, El-Sayed MA. Small molecule-gold nanorod conjugates selectively target and induce macrophage cytotoxicity towards breast cancer cells. Small 2012;8:2819–22.
[24] Zhu SJ, Niu MM, O'Mary H, Cui ZR. Targeting of tumor-associated macrophages made possible by PEG-sheddable, mannose-modified nanoparticles. Mol Pharm 2013;10:3525–30.
[25] VanHandel M, Alizadeh D, Zhang L, Kateb B, Bronikowski M, Manohara H, et al. Selective uptake of multi-walled carbon nanotubes by tumor macrophages in a murine glioma model. J Neuroimmunol 2009;208:3–9.
[26] Alizadeh D, Zhang L, Hwang J, Schluep T, Badie B. Tumor-associated macrophages are predominant carriers of cyclodextrin-based nanoparticles into gliomas. Nanomedicine: Nanotechnol Biol Med 2010;6:382–90.
[27] Lesniak W, Mishra MK, Jyoti A, Balakrishnan B, Zhang F, Nance E, et al. Biodistribution Fluorescently-labeled PAMAM Dendrimers Neonatal Rabbits: Eff Neuroinflammation. Mol Pharm 2013.
[28] Recinos VR, Tyler BM, Bekelis K, Sunshine SB, Vellimana A, Li KW, et al. Combination of intracranial temozolomide with intracranial carmustine improves survival when compared with either treatment alone in a rodent glioma model. Neurosurgery 2010;66:530–7. discussion 7.
[29] Venishetty VK, Komuravelli R, Kuncha M, Sistla R, Diwan PV. Increased brain uptake of docetaxel and ketoconazole loaded folate-grafted solid lipid nanoparticles. Nanomedicine (Lond) 2013;9:111–21.
[30] Shankar R, Samykutty A, Riggin C, Kannan S, Wenzel U, Kolhatkar R. Cathepsin B degradable star-shaped peptidic macromolecules for delivery of 2-methoxyestradiol. Mol Pharm 2013;10:3776–88.
[31] Orr AG, Orr AL, Li XJ, Gross RE, Traynelis SF. Adenosine A(2A) receptor mediates microglial process retraction. Nat Neurosci 2009;12:872–8.
[32] Dinda AK, Sarkar C, Roy S, Kharbanda K, Mathur M, Khosla AK, et al. A transmission and scanning electron microscopic study of tumoral and peritumoral microblood vessels in human gliomas. J Neuro-oncol 1993;16:149–58.
[33] Choi M, Choi K, Ryu SW, Lee J, Choi C. Dynamic fluorescence imaging for multiparametric measurement of tumor vasculature. J Biomed Opt 2011;16.046008.
[34] Komohara Y, Ohnishi K, Kuratsu J, Takeya M. Possible involvement of the M2 anti-inflammatory macrophage phenotype in growth of human gliomas. J Pathol 2008;216:15–24.
[35] Badie B, Schartner J. Role of microglia in glioma pathology. Microsc Res Tech 2001:106–13.
[36] Roggendorf W, Strupp S, Paulus W. Distribution and characterization of microglia/macrophages in human brain tumors. Acta Neuropathol 1996;92:288–93.
[37] Hussain SF, Yang D, Suki D, Aldape K, Grimm E, Heimberger AB. The role of human glioma-infiltrating microglia/macrophages in mediating antitumor immune responses. Neuro-oncology 2006;8:261–79.
[38] Boche D, Perry VH, Nicoll JA. Review: activation patterns of microglia and their identification in the human brain. Neuropathology Appl Neurobiol 2013;39:3–18.
[39] Sadekar S, Linares O, Noh G, Hubbard D, Ray A, Janat-Amsbury M, et al. Comparative pharmacokinetics of PAMAM-OH dendrimers and HPMA copolymers in ovarian-tumor-bearing mice. Drug Deliv Transl Res 2013;3:260–71.
[40] Wohlfart S, Khalansky AS, Gelperina S, Begley D, Kreuter J. Kinetics of transport of doxorubicin bound to nanoparticles across the blood-brain barrier. J Controlled Release: Off J Control Release Soc 2011;154:103–7.
[41] Noell S, Mayer D, Strauss WSL, Tatagiba MS, Ritz R. Selective enrichment of hypericin in malignant glioma: pioneering in vivo results. Int J Oncol 2011;38:1343–8.
[42] Dave N, Gudelsky GA, Desai PB. The pharmacokinetics of letrozole in brain and brain tumor in rats with orthotopically implanted C6 glioma, assessed using intracerebral microdialysis. Cancer Chemother Pharmacol 2013;72:349–57.
[43] Wu W, Driessen W, Jiang X. Oligo(ethylene glycol)-based thermosensitive dendrimers and their tumor accumulation and penetration. J Am Chem Soc 2014;136:3145–55.
[44] Lee CC, Gillies ER, Fox ME, Guillaudeu SJ, Frechet JM, Dy EE, et al. A single dose of doxorubicin-functionalized bow-tie dendrimer cures mice bearing C-26 colon carcinomas. Proc Natl Acad Sci U S A 2006;103:16649–54.
[45] Meyers JD, Doane T, Burda C, Basilion JP. Nanoparticles for imaging and treating brain cancer. Nanomedicine (Lond) 2013;8:123–43.
[46] Brigger I, Morizet J, Laudani L, Aubert G, Appel M, Velasco V, et al. Negative preclinical results with stealth nanospheres-encapsulated doxorubicin in an orthotopic murine brain tumor model. J Control Release: Off J Control Release Soc 2004;100:29–40.
[47] Arnold RD, Mager DE, Slack JE, Straubinger RM. Effect of repetitive administration of doxorubicin-containing liposomes on plasma pharmacokinetics and drug biodistribution in a rat brain tumor model. Clin Cancer Res 2005;11:8856–65.
[48] Chertok B, David AE, Moffat BA, Yang VC. Substantiating in vivo magnetic brain tumor targeting of cationic iron oxide nanocarriers via adsorptive surface masking. Biomaterials 2009;30:6780–7.
[49] Siegal T. Which drug or drug delivery system can change clinical practice for brain tumor therapy? Neuro-oncol 2013;15:656–69.
[50] Chauhan VP, Jain RK. Strategies for advancing cancer nanomedicine. Nat Mater 2013;12:958–62.
[51] Perrault SD, Walkey C, Jennings T, Fischer HC, Chan WCW. Mediating tumor targeting efficiency of nanoparticles through design. Nano Lett 2009;9:1909–15.
[52] Wang K, Zhang X, Liu Y, Liu C, Jiang B, Jiang Y. Tumor penetrability and anti-angiogenesis using iRGD-mediated delivery of doxorubicin-polymer conjugates. Biomaterials 2014;35:8735–47.

[53] Nance E, Zhang C, Shih TY, Xu Q, Schuster BS, Hanes J. Brain-penetrating nanoparticles improve paclitaxel efficacy in malignant glioma following local administration. ACS Nano 2014;8:10655–64.
[54] Yoshii Y, Sugiyama K. Intercapillary distance in the proliferating area of human glioma. Cancer Res 1988;48:2938–41.
[55] Choi HS, Liu W, Misra P, Tanaka E, Zimmer JP, Ipe BI, et al. Renal clearance of quantum dots. Nat Biotechnol 2007;25:1165–70.
[56] Kobayashi H, Kawamoto S, Jo SK, Sato N, Saga T, Hiraga A, et al. Renal tubular damage detected by dynamic micro-MRI with a dendrimer-based magnetic resonance contrast agent. Kidney Int 2002;61:1980–5.
[57] Curthoys NP, Moe OW. Proximal tubule function and response to acidosis. Clin J Am Soc Nephrol: CJASN 2013.
[58] Kannan RM, Nance E, Kannan S, Tomalia DA. Emerging concepts in dendrimer-based nanomedicine: from design principles to clinical applications. J Intern Med 2014;276:579–617. http://dx.doi.org/10.1111/joim.12280.